Giant Viscoelasticity near Mott Criticality in $PbCrO_3$ with Large Lattice Anomalies

Shanmin Wang,* Jian Chen, Liusuo Wu, and Yusheng Zhao
Department of Physics and Academy for Advanced Interdisciplinary Studies, Southern University of Science and Technology, Shenzhen, Guangdong 518055, China

(Received 25 September 2020; revised 17 December 2021; accepted 7 February 2022; published 4 March 2022)

Coupling of charge and lattice degrees of freedom in materials can produce intriguing electronic phenomena, such as conventional superconductivity where the electrons are mediated by lattice for creating supercurrent. The Mott transition, which is a source for many fascinating emergent behaviors, is originally thought to be driven solely by correlated electrons with an Ising criticality. Recent studies on the known Mott systems have shown that the lattice degree of freedom is also at play, giving rise to either Landau or unconventional criticality. However, the underlying coupling mechanism of charge and lattice degrees of freedom around the Mott critical end point remains elusive, leading to difficulties in understanding the associated Mott physics. Here, we report a study of Mott transition in cubic $PbCrO_3$ by measuring the lattice parameter, using high-pressure x-ray diffraction techniques. The Mott criticality in this material is revealed with large lattice anomalies, which is governed by giant viscoelasticity that presumably results from a combination of lattice elasticity and electron viscosity. Because of the viscoelastic effect, the lattice of this material behaves peculiarly near the critical end point, inconsistent with any existing university classes. We argue that the viscoelasticity may play as a hidden degree of freedom behind the Mott criticality.

DOI: 10.1103/PhysRevLett.128.095702

Introduction.—The correlated electrons in materials can condense into new forms of collective states by varying pressure (P) and temperature (T), and they are a key to many emergent phenomena, such as unconventional superconductivity [1], spin-liquid phases [2], and quantum criticality [1–3]. Understanding these phenomena is closely linked to the Mott insulator-metal transition that is mainly characterized by a first-order isostructural transition ended at a second-order critical end point in the associated P-T space [4]. Critical properties of a Mott system are expected to be described in the framework of the scaling theory of a known universality class [5,6], allowing gaining insights into collective nature of the system.

The first experimental determination of Mott critical behaviors comes to the Cr-doped V_2O_3 by conductivity measurements, revealing an Ising criticality [6], and it can be understood in terms of the classical liquid-gas transition, indicating a purely electronic system [7,8]. However, slightly away from the end point of this system, the Landau criticality is favored, due to the effect of lattice deformation on its electronic system [7]. Intriguingly, an unconventional criticality in an organic salt κ-$(BEDT\text{-}TTF)_2Cu[N(CN)_2]Cl$ (denoted by κ-Cl hereafter) was also found [9,10], which is distinct from any existing universality classes. According to Zacharias *et al.* [7], incorporating the lattice elasticity into a purely electronic critical state can lead to the suppression of microscopic charge fluctuation by the long-ranged shear stress, which explains the crossover from Ising to either Landau or unconventional criticality with a more rapid ordering of the charge degree of freedom [9]. However, the underlying charge-lattice coupling mechanism for the Mott criticality is still unclear.

Intuitively, the lattice seemingly functions as a glue for mediating electrons to form new collective states around the critical end point, similar to the mechanism for forming Cooper pairs in conventional superconductors [11]. Such new electronic states should have viscosity due to the frequent electron-electron collisions, as the thermally induced scattering by the lattice is completely suppressed. In fact, the electron viscosity has been revealed by a surge of recent experiments [12–15], although it was originally predicted by Landau [12]. The thus-produced electron viscosity combined with lattice elasticity would produce viscoelasticity in the associated materials. Materials with viscoelastic properties are expected to exhibit many mechanical anomalies [16–18], which can explain the Mott critical behaviors.

The lattice strain can thus provide a straightforward probe for exploring the viscoelastic effect. Using both the ultrasound and dilatometric measurements, a large elastic softening in Cr-doped V_2O_3 [19,20] and anomalous thermal expansions in κ-Cl were previously reported around their critical end points [21]. A recent isothermal dilatometric experiment on κ-Cl has led to a successful study of its Mott criticality by monitoring the macroscopic sample length [8], but it suffers from complicated data analysis as multiple strain components are involved. By contrast,

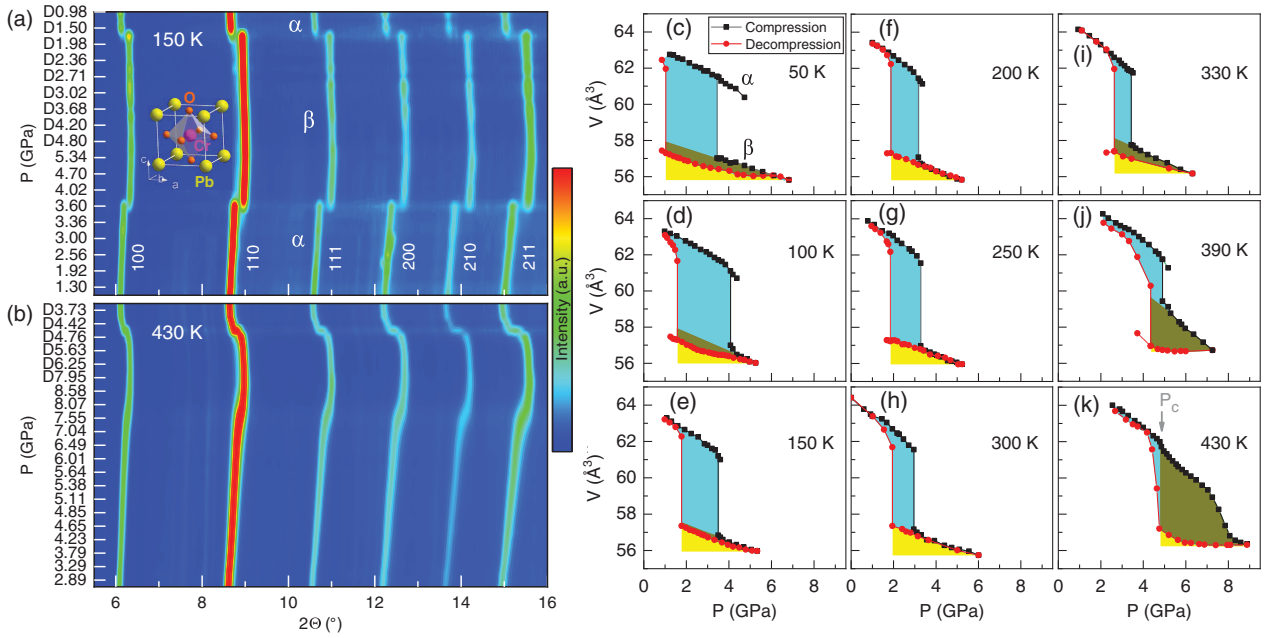

FIG. 1. Isothermal high-P XRD patterns and P-V data for $PbCrO_3$. (a),(b) Contour plots of high-P XRD patterns collected upon both compression and decompression ("D") at 150 and 430 K, respectively. Inset is the unit cell. The incident x-ray wavelength is $\lambda = 0.4246$ Å. (c)–(k) Isothermal P-V data. In each panel, the cyan, dark yellow, and yellow shaded regions correspond to the phase-transition hysteresis loss, viscoelastic dissipation, and recoverable elastic energy, respectively. The error bars are too small to show.

high-P x-ray diffraction (XRD) combined with a precise temperature control is a powerful tool to look into the Mott transition by probing lattice parameters under varying P-T conditions [22,23]. The expected critical elastic anomalies can thus be explored by volumetric (V) analysis. However, the known Mott systems with low critical pressures (i.e., below 1 GPa) are unfavorable for high-P XRD experiment. In this regard, as a recently identified Mott system $PbCrO_3$ is suitable with a moderate critical pressure of ~3 GPa [24]. Besides, conflicting mechanisms of charge disproportionation [25] and melting of charge glass [26] were also proposed for explaining pressure-induced isostructural transition in this oxide [27], and ambiguities of its magnetic, electronic, and ferroelectric properties still remain [24–34], calling for more experimental efforts. Here, we present a systematic high-P study of $PbCrO_3$ with a focus on its lattice Mott criticality (see Supplemental Material for experimental details [35]), leading to the discovery of giant viscoelasticity around its critical end point. Based on the viscoelastic effect, the observed elastic anomalies and unconventional lattice criticality can be well interpreted, shedding light on the underlying mechanism of Mott transition.

Results and discussion.—High-P XRD patterns of $PbCrO_3$ taken during isothermal loading cycles are shown in Figs. 1(a) and 1(b) (see Figs. S1–S11 for detailed data analysis and structural refinements [36]). For simplicity, the low-P insulating and high-P metallic phases are hereafter denoted with α and β, respectively [24]. Below 390 K, the pressure-induced $\alpha \rightarrow \beta$ transition is primarily characterized by a remarkable shift of each of the involved diffraction peaks without the appearance of additional peaks, suggesting a first-order isostructural transition [Fig. 1(a)], consistent with previous reports [24,25,27]. However, at 430 K the forward α-β transition becomes a second order without sharp peak shifts [Fig. 1(b)], and the transition pressure is hardly discerned from the peak shift. Upon decompression, the reverse transition can still be identified by peak shifts at ~4.8 GPa, although the shifts are continuous. Besides, a prominent peak broadening is occurred above 4 GPa and reaches maximum around 7.6 GPa with a rapid lattice softening [Fig. 1(b) and Fig. S11], due to the viscoelastic effect as discussed later.

Figures 1(c)–1(k) present the obtained high-P isothermal volume data of $PbCrO_3$. In each loading cycle, a hysteresis loop can be defined by both the forward and reverse thresholds. Clearly, the loop area is equal to an energy dissipation related to the structural transition kinetics [37,38]. With increasing temperatures, the pressure hysteresis progressively decreases, especially above 300 K, which eventually vanishes at a critical temperature (T_c) of ~430 K [Fig. 1(k)]; similar hysteresis can also be identified from the variation of phase fraction (Fig. S8). In each isothermal P-V line of β-$PbCrO_3$ below 150 K and above 300 K, a deviation appears between the compression and decompression processes, leading to an extra P-V loop, a characteristic of viscoelastic behaviors [39]. Note that the viscoelastic effect can only appear in the β phase with delocalized electrons and likely results from a combination of electron viscosity and lattice elasticity. The

thus-produced extra loop area corresponds to an additional energy dissipation, due to the viscoelastic deformation. Recoverable elastic energy in β-$PbCrO_3$ can be integrated from its decompression P-V curve. With decreasing temperature below 150 K, such a viscoelastic loop is enlarged with reducing recoverable elasticity, indicating enhanced viscoelasticity [Figs. 1(c) and 1(d)]. Interestingly, the loop area promptly grows above 300 K. At T_c, the viscoelastic deformation prevails, leading to a huge amount of energy dissipation and nearly zero recoverable energy. In contrast, at 200–300 K the β phase exhibits a purely elastic nature without involvement of viscoelastic loop [Figs. 1(f)–1(h)].

On a close look at the forward transition at T_c [Fig. 2(a)], a remarkably different lattice behavior starts from 4.82 GPa. Coincidently, the reverse transition occurs at the nearly same pressure during decompression, indicating a critical pressure (P_c) of ~4.82 GPa. The thus-determined Mott critical end point for $PbCrO_3$ is at $T_c \approx 430$ K and $P_c \approx 4.82$ GPa. Because of the viscoelastic effect, the volume reduction in forward transition is suppressed, resulting in a second-order transition. However, a prompt volume contraction above 7 GPa may indicate a rapidly varying viscoelasticity with anomalous peak broadening, especially around 7.6 GPa [Fig. 1(b)]. Above 8 GPa, the lattice of β-$PbCrO_3$ has a normal stiffness (i.e., $B_0 \approx 113$), close to that at 300 K with pure elasticity, whereas it remains nearly invariant during decompression till the reverse transition, implying viscoelasticity-induced anomalies in elasticity. On the removal of pressure, β-$PbCrO_3$ can fully recover to its original phase with characteristics of anelasticity, a special case of viscoelasticity [40].

Based on these experimental observations, a P-T phase diagram of $PbCrO_3$ is depicted in Fig. 2(b). Apparently, the

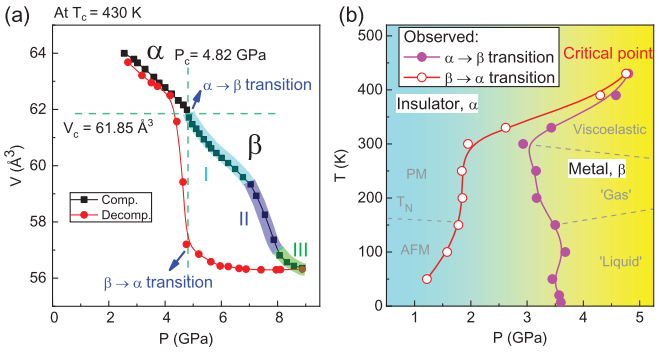

FIG. 2. Lattice Mott criticality near the end point (P_c, T_c) and phase diagram of $PbCrO_3$. (a) P-V data at $T_c = 430$ K. Compression P-V line of β can be divided into three different regions of I, II, and III, as highlighted in cyan, blue, and green, respectively. (b) P-T phase diagram. The two spinodal lines are defined by the forward and reverse α-β thresholds. The delocalized electrons in β-$PbCrO_3$ have three different states of "liquid," "gas," and viscoelastic state. Paramagnetic (PM)-to-antiferromagnetic (AFM) transition line (T_N) determined by high-P neutron diffraction will be published elsewhere.

P-T space is mainly divided into three regions by two spinodal lines, including insulating α, metallic β, and two-phase coexistence regions. The two spinodal lines are constrained by first-order transition lines, terminating in a critical end point (T_c, P_c), beyond which the transition is second order. The similar phase diagrams have been observed in other Mott systems (e.g., Cr-doped V_2O_3 [4,6] and κ-Cl [41,42]). In the β region, the delocalized electrons may have three distinct states of "liquid," "gas," and viscoelastic state as discussed later; such a picture is reminiscent of water with liquid, gas, and supercritical fluid states under P-T conditions [5]. Interestingly, the shape of two spinodal lines is seemingly affected by these electronic states. In particular, the sharpening of two-phase coexistence region coincidently occurs in the vicinity of appearance of viscoelasticity above 300 K. Besides, the superlarge viscoelasticity is expected at (T_c, P_c). Thus, coupling of lattice elasticity and electron viscosity in β-$PbCrO_3$ could generate giant viscoelasticity, which ultimately governs the Mott critical properties.

For a Mott system, the critical exponents of observable quantities around the critical end point is important, based on which the transition can be classified and understood within the framework of the scaling theory of classical systems [5]. To extract the Mott critical exponents for $PbCrO_3$, the relative lattice densities $|\rho$-$\rho_c|$ of both the insulating and metallic phases at 430 K are plotted in Fig. 3(a) as a function of pressure, $|P$-$P_c|$, obeying the same power law $|P$-$P_c|^{1/\delta}$ with $\delta \approx 4/3$. On the border of coexistence region, the variation of relative density of the metallic phase (ρ_{metal}-ρ_c) against temperature (T_c-T) is shown in Fig. 3(b). Using the scaling relation $(T_c$-$T)^{\beta}$, the best fit can be achieved for only the high-T region (i.e., 300–430 K) with $\beta \approx 3/5$. Therefore, the obtained critical exponents are $(\delta, \beta) \approx (4/3, 3/5)$ [Fig. 3(c)], inconsistent with those of existing universality classes (i.e., $\delta \geq 3$ and $\beta \leq 1/2$) bounded by the mean-field values of $(\delta, \beta) = (3, 1/2)$ or the well-studied Mott systems [e.g., $(V_{1-x}Cr_x)_2O_3$ [6] and organic κ-Cl [9,10]].

Remarkably, $PbCrO_3$ exhibits unconventional critical behaviors, which can be understood in terms of the viscoelastic effect, indicating that the real order parameter of this system may be viscoelasticity, rather than the pure charge or lattice degree of freedom. The viscoelasticity is closely related to the high-P metallic phase and should originate from a synthesis of electron viscosity and lattice elasticity. The relative ratio between these two components could be changed in different systems, leading to distinctly different critical behaviors. From this viewpoint, the viscous component in $(V_{1-x}Cr_x)_2O_3$ is likely dominated, because its critical behaviors obey the mean-field and 3D models [Fig. 3(c)] [6]. However, the Mott criticalities in $PbCrO_3$ and κ-Cl probably involve large fractions of elastic component [9,10], which results in unconventional critical exponents far beyond the limit of conventional classes, giving rise to more rapid orderings of order parameters.

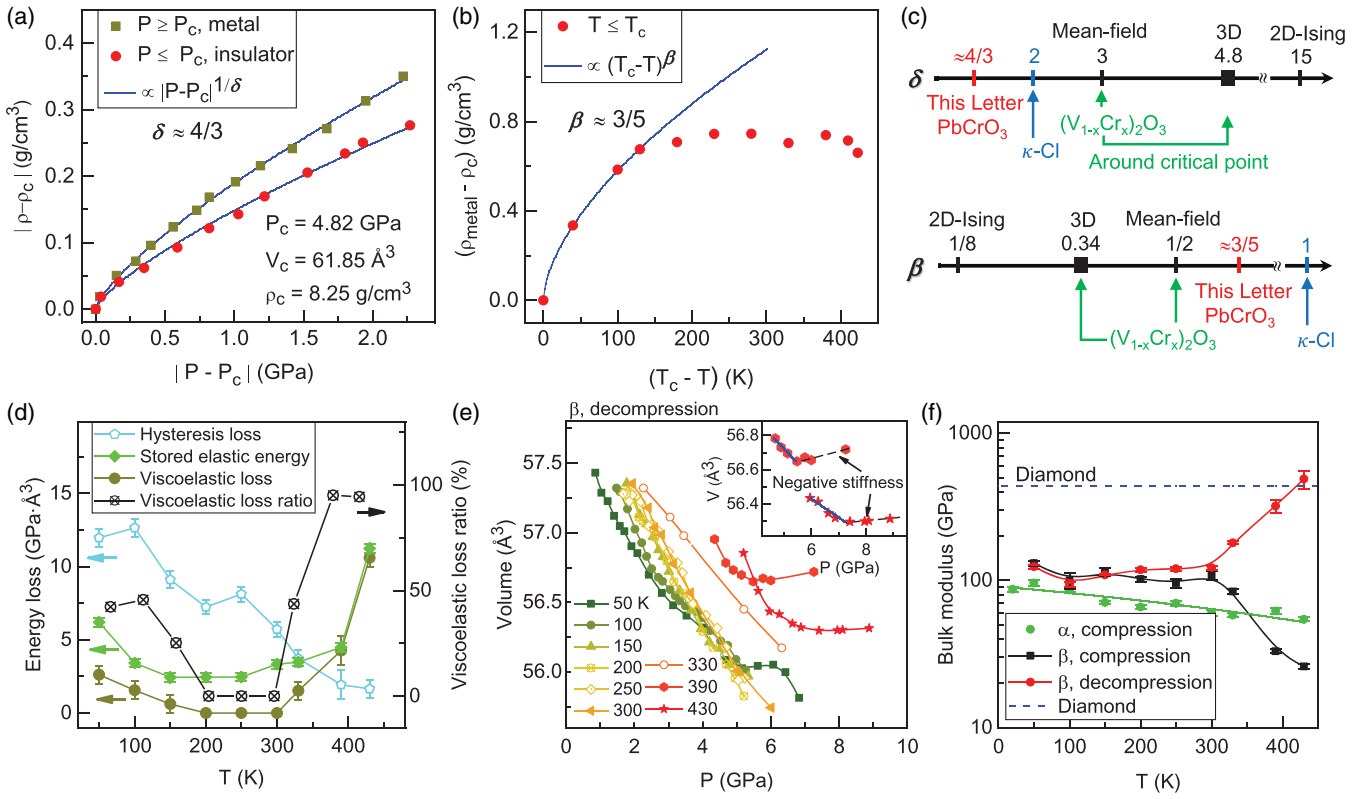

FIG. 3. Mott critical behaviors, energy dissipation, and viscoelastic stiffness. (a) Lattice density vs pressure. (b) Lattice density vs temperature for metallic phase on the border of coexistence region. (c) Comparison of critical exponents of $PbCrO_3$ with those of universality (e.g., mean-field, 2D-Ising, and 3D models [9]). Critical exponents of $(V_{1-x}Cr_x)_2O_3$ and κ-Cl are added [6,9]. (d) Total elastic energy storage in β-$PbCrO_3$, viscoelastic and hysteresis dissipations, and the ratio of viscoelastic loss to the stored elastic energy vs temperature derived from integrations of the P-V data [Figs. 1(c)–1(k) and Fig. S12]. The total elastic energy is the sum of viscoelastic and recoverable elastic energies. (e) Isothermal P-V data for β-$PbCrO_3$ collected during decompression. The inset is an enlarged portion of the cases at 390 and 430 K. Each blue line represents a fit of the associated isothermal P-V data to a second-order Birch-Murnaghan EOS. (f) Isothermal bulk moduli for both α- and β-$PbCrO_3$.

To quantitatively explore the viscoelastic effect, we derive the associated energy dissipations and the totally stored and recoverable elastic energies in the β phase by integrating the P-V areas [Fig. 3(d) and Fig. S12]. As expected, the hysteresis-induced energy dissipation progressively reduces to zero, as the T_c is approached. By contrast, the viscoelastic dissipation is small at 50 K and gradually decreases to zero at 200–300 K, followed by a rapid increase at 330–430 K. In fact, the viscoelasticity can be quantified by the ratio of viscoelastic energy to total elastic energy storage in β-$PbCrO_3$ during compression. Around T_c, nearly all the stored elastic energy is dissipated by the viscoelastic deformation, producing a giant viscoelastic effect. During decompression, the lattice of β-$PbCrO_3$ exhibit complex responses to these energy variations [Fig. 3(e) and Figs. S13–S14]. At 50 K, clear lattice anomalies occur at 3–7 GPa and progressively diminish at 200 K. In the 200–300 K range, the isothermal volume data has a similar linear variation with pressure, which can be well described by the Birch-Murnaghan equation of state (EOS) [43], in striking contrast to that around T_c with large lattice anomalies.

Considering no structural change is involved, these phenomena can only be associated with delocalized electrons in β-$PbCrO_3$, which could have distinct collective states with varying temperature, hence different viscosities [12]. It is speculated that a liquidlike state occurs below 150 K with certain viscosity, because the electrons are weakly scattered by the lattice at low temperatures. At 200–300 K, the electrons may be frequently scattered by the lattice, so that the electron-electron collisions are hindered, leading to the formation of a nonviscous gaslike state. In this case, the interplay between the electrons and lattice elasticity is weak, which is responsible for its normal elastic behaviors [Figs. 1(f)–1(h)]. However, the viscoelastic effect is counterintuitively increased above 300 K, inferring an unusual mechanism for the formation of large electron viscosity. As mentioned earlier, the delocalized electrons are likely glued by the lattice to form viscous flow, and the viscosity increases upon approaching to T_c, which may even lead to superviscosity at the critical end point. Such viscous electrons can react with the lattice to form viscoelasticity in β-$PbCrO_3$ in the 50–150 K and 330–430 K ranges, causing lattice anomalies. Above 390 K,

because of the super-large viscoelasticity, the negative stiffness occurs in the β phase with positive slopes at the early stage of decompression (i.e., volume shrinking upon decompression) [Fig. 3(e)].

In principle, a material with negative stiffness is unstable, unless it is predeformed (i.e., containing stored energy) and constrained by a soft surrounding matrix to form inclusion-matrix composite [16–18,44–46]. Negative stiffness can produce extreme physical properties in the composite including giant damping, time-dependent strain, and extremely high dynamic elastic modulus [18,47], as observed in the Sn-included $BaTiO_3$ and VO_2 composites [16,18]. Obviously, β-$PbCrO_3$ is a high-P metallic phase with a prestrained volume; around the critical end point, the delocalized electrons would form a superviscous fluid that plays as a soft "matrix," satisfying the prerequisites for producing negative stiffness. Besides, the expected extremely large dynamic bulk modulus (B_0) of $PbCrO_3$ are also observed [Fig. 3(f)]. Below 300 K, the bulk modulus of β phase is leveled off at ~120 GPa, irrespective of compression or decompression; however, above 300 K it increases exponentially and reaches ~490 GPa at T_c during decompression [Fig. 3(f) and Fig. S14], which is even substantially greater than that of diamond (i.e., 440 GPa). For the cases obtained during compression, the trend is reversed and the bulk modulus is exponentially decreased (e.g., only ~26 GPa at T_c). These elastic anomalies can be well explained according to the viscoelastic effect. However, for the insulating α phase the derived B_0 decreases linearly without involving any anomalies [Fig. 3(f)], because there is no itinerant electron in this phase for producing electron viscosity. Because of the viscoelastic damping, the lattice strain in β-$PbCrO_3$ is dynamic in nature, which should be out of phase from the stress or applied pressure (e.g., the strain lags behind the stress), especially near the criticality. One of the remarkable consequences is that the sharp volume change is suppressed across the phase transition, resulting in a crossover from the first to second order transition. Last, using our recently developed high-P technique, we performed dynamic high-P transport experiments [48], leading to the observation of a time-dependent effect of lattice contraction on the electrical resistance of β-$PbCrO_3$, which is probably associated with the viscoelasticity (Fig. S16).

In summary, by the high-P isothermal volumetric measurement, the Mott transition and lattice Mott criticality in $PbCrO_3$ are systematically investigated. The P-T phase diagram of this Mott system is well mapped out by two first-order-transition spinodal lines, terminating in a second-order critical end point at $T_c \approx 430$ K and $P_c \approx 4.82$ GPa. Close to the critical temperature, giant viscoelasticity is revealed in the high-P metallic phase, which is presumably a combined result of electrons viscosity and lattice elasticity. Based on the viscoelastic effect, a number of anomalous critical properties of this system can be well interpreted, including unusual Mott criticality, anomalous lattice behaviors, negative stiffness, and extremely high dynamic bulk modulus. In addition, our results would also be applicable to understanding the relevant problems, such as high-T superconductivity where the viscoelastic effect may be decisive.

The data that support the findings of this study are available from the corresponding authors upon reasonable request.

This work is supported by the National Natural Science Foundation of China (Grant No. 12174175 and No. 12134020), the Key Research Platforms and Research Projects of Universities in Guangdong Province (Grant No. 2018KZDXM062), the Guangdong Innovative & Entrepreneurial Research Team Program (No. 2016ZT06C279), the Shenzhen Peacock Plan (No. KQTD2016053019134356), the Shenzhen Development and Reform Commission Foundation for Shenzhen Engineering Research Center for Frontier Materials Synthesis at High Pressure, the Shenzhen Key Laboratory of Advanced Quantum Functional Materials and Devices (Grant No. ZDSYS20190902092905285), and the Research Platform for Crystal Growth & Thin-Film Preparation at SUSTech. High-P synchrotron XRD experiments were performed at the 16-BMD beamline of HPCAT/APS. We thank B. Hou, C. Park, and C. Kenney-Benson for their help on the setup of high-P synchrotron experiments at HPCAT.

The authors declare no competing interests.

*wangsm@sustech.edu.cn

[1] M. Imada, A. Fujimori, and Y. Tokura, Rev. Mod. Phys. **70**, 1039 (1998).
[2] L. Balents, Nature (London) **464**, 199 (2010).
[3] T. Furukawa, K. Miyagawa, H. Taniguchi, R. Kato, and K. Kanoda, Nat. Phys. **11**, 221 (2015).
[4] D. Jerome, Nat. Phys. **5**, 864 (2009).
[5] L. P. Kadanoff, W. Götze, D. Hamblen, R. Hecht, E. A. S. Lewis, V. V. Palciauskas, M. Rayl, J. Swift, D. Aspnes, and J. Kane, Rev. Mod. Phys. **39**, 395 (1967).
[6] P. Limelette, A. Georges, D. Jérome, P. Wzietek, P. Metcalf, and J. M. Honig, Science **302**, 89 (2003).
[7] M. Zacharias, L. Bartosch, and M. Garst, Phys. Rev. Lett. **109**, 176401 (2012).
[8] E. Gati, M. Garst, R. S. Manna, U. Tutsch, B. Wolf, L. Bartosch, H. Schubert, T. Sasaki, J. A. Schlueter, and M. Lang, Sci. Adv. **2**, e1601646 (2016).
[9] F. Kagawa, K. Miyagawa, and K. Kanoda, Nature (London) **436**, 534 (2005).
[10] F. Kagawa, K. Miyagawa, and K. Kanoda, Nat. Phys. **5**, 880 (2009).
[11] M. R. Norman, Science **332**, 196 (2011).
[12] M. Polini and A. K. Geim, Phys. Today **73**, 28 (2020).

[13] A. I. Berdyugin, S. G. Xu, F. M. D. Pellegrino, R. Krishna Kumar, A. Principi, I. Torre, M. Ben Shalom, T. Taniguchi, K. Watanabe, I. V. Grigorieva, M. Polini, A. K. Geim, and D. A. Bandurin, Science **364**, 162 (2019).
[14] P. J. W. Moll, P. Kushwaha, N. Nandi, B. Schmidt, and A. P. Mackenzie, Science **351**, 1061 (2016).
[15] L. Levitov and G. Falkovich, Nat. Phys. **12**, 672 (2016).
[16] T. Jaglinski, D. Kochmann, D. Stone, and R. S. Lakes, Science **315**, 620 (2007).
[17] R. S. Lakes, Phys. Rev. Lett. **86**, 2897 (2001).
[18] R. S. Lakes, T. Lee, A. Bersie, and Y. C. Wang, Nature (London) **410**, 565 (2001).
[19] S. Populoh, P. Wzietek, R. Gohier, and P. Metcalf, Phys. Rev. B **84**, 075158 (2011).
[20] S. R. Hassan, A. Georges, and H. R. Krishnamurthy, Phys. Rev. Lett. **94**, 036402 (2005).
[21] M. de Souza, A. Brühl, C. Strack, B. Wolf, D. Schweitzer, and M. Lang, Phys. Rev. Lett. **99**, 037003 (2007).
[22] S. V. Sinogeikin, J. S. Smith, E. Rod, C. Lin, C. Kenney-Benson, and G. Shen, Rev. Sci. Instrum. **86**, 072209 (2015).
[23] H. K. Mao, J. Xu, and P. M. Bell, J. Geophys. Res. **91**, 4673 (1986).
[24] S. Wang, J. Zhu, Y. Zhang, X. Yu, J. Zhang, W. Wang, L. Bai, J. Qian, L. Yin, N. S. Sullivan, C. Jin, D. He, J. Xu, and Y. Zhao, Proc. Natl. Acad. Sci. U.S.A. **112**, 15320 (2015).
[25] J. Cheng, K. E. Kweon, S. A. Larregola, Y. Ding, Y. Shirako, L. G. Marshall, Z.-Y. Li, X. Li, A. M. dos Santos, M. R. Suchomel, K. Matsubayashi, Y. Uwatoko, G. S. Hwang, J. B. Goodenough, and J.-S. Zhou, Proc. Natl. Acad. Sci. U.S.A. **112**, 1670 (2015).
[26] R. Yu *et al.*, J. Am. Chem. Soc. **137**, 12719 (2015).
[27] W. Xiao, D. Tan, X. Xiong, J. Liu, and J. Xu, Proc. Natl. Acad. Sci. U.S.A. **107**, 14026 (2010).
[28] W. L. Roth and R. C. DeVries, J. Appl. Phys. **38**, 951 (1967).
[29] Á. M. Arévalo-López and M. Á. Alario-Franco, J. Solid State Chem. **180**, 3271 (2007).
[30] B. L. Chamberland and C. W. Moeller, J. Solid State Chem. **5**, 39 (1972).
[31] Y. Lu, D. He, F. Peng, and X. Cheng, Eur. Phys. J. B **86**, 352 (2013).
[32] W.-D. Wang, D.-W. He, W.-S. Xiao, S.-M. Wang, and J.-A. Xu, Chin. Phys. Lett. **30**, 117201 (2013).
[33] Á. M. Arévalo-López, A. J. Dos santos-García, and M. A. Alario-Franco, Inorg. Chem. **48**, 5434 (2009).
[34] B.-T. Wang, W. Yin, W.-D. Li, and F. Wang, J. Appl. Phys. **111**, 013503 (2012).
[35] See Supplemental Material at http://link.aps.org/supplemental/10.1103/PhysRevLett.128.095702 for experimental details, isothermal high-P XRD patterns, structural refinement and XRD data analysis, bulk modulus analysis, and dynamic high-P resistance measurements.
[36] B. H. Toby, J. Appl. Crystallogr. **34**, 210 (2001).
[37] U. D. Venkateswaran, L. J. Cui, B. A. Weinstein, and F. A. Chambers, Phys. Rev. B **45**, 9237 (1992).
[38] X. Yan, X. Ren, S. Zhu, D. Van Gennep, L. Wang, Y. Zhao, and S. Wang, Phys. Rev. B **103**, L140103 (2021).
[39] M. A. Meyers and K. K. Chawla, *Mechanical Behavior of Materials* (Cambridge University Press, Cambridge, England, 2009).
[40] W. Benoit, in *Encyclopedia of Condensed Matter Physics*, edited by F. Bassani, G. L. Liedl, and P. Wyder (Elsevier, Oxford, 2005), p. 271.
[41] P. Limelette, P. Wzietek, S. Florens, A. Georges, T. A. Costi, C. Pasquier, D. Jérome, C. Mézière, and P. Batail, Phys. Rev. Lett. **91**, 016401 (2003).
[42] S. Lefebvre, P. Wzietek, S. Brown, C. Bourbonnais, D. Jérome, C. Mézière, M. Fourmigué, and P. Batail, Phys. Rev. Lett. **85**, 5420 (2000).
[43] F. Birch, Phys. Rev. **71**, 809 (1947).
[44] W. J. Drugan, Phys. Rev. Lett. **98**, 055502 (2007).
[45] C. S. Wojnar and D. M. Kochmann, Philos. Mag. **94**, 532 (2014).
[46] R. H. Baughman, J. M. Shacklette, A. A. Zakhidov, and S. Stafström, Nature (London) **392**, 362 (1998).
[47] R. Lakes and K. W. Wojciechowski, Phys. Status Solidi (b) **245**, 545 (2008).
[48] J. Chen, H. Cheng, X. Zhou, X. Yan, L. Wang, Y. Zhao, and S. Wang, Rev. Sci. Instrum. **92**, 033905 (2021).